Silicon Nanowire-Based Molecular Beacons for High-Sensitivity and Sequence-Specific DNA Multiplexed Analysis

Shao Su,[†,§] Xinpan Wei,[†] Yiling Zhong,[†] Yuanyuan Guo,[†] Yuanyuan Su,[†] Qing Huang,[§] Shuit-Tong Lee,[‡,*] Chunhai Fan,[§,*] and Yao He[†,*]

[†]Institute of Functional Nano & Soft Materials (FUNSOM) and Jiangsu Key Laboratory for Carbon-Based Functional Materials & Devices, Soochow University, Suzhou 215123, China, [‡]Center of Super-Diamond & Advanced Films (COSDAF) and Department of Physics & Materials Science, City University of Hong Kong, Hong Kong SAR, China, and [§]Laboratory of Physical Biology, Shanghai Institute of Applied Physics, Chinese Academy of Sciences, Shanghai 201800, China

ABSTRACT

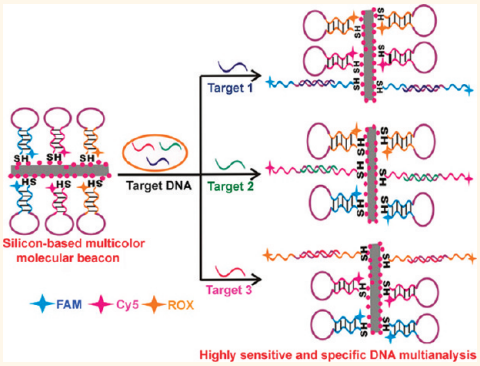

Nanomaterial-based molecular beacons (nanoMBs) have been extensively explored due to unique merits of nanostructures, including gold nanoparticle (AuNP)-, carbon nanotube (CNT)-, and graphene-based nanoMBs. Those nanoMBs are well-studied; however, they possess relatively poor salt stability or low specificity, limiting their wide applications. Here, we present a novel kind of multicolor silicon-based nanoMBs by using AuNP-decorated silicon nanowires as high-performance quenchers. Significantly, the nanoMBs feature robust stability in high-concentration (0.1 M) salt solution and wide-ranging temperature (10−80 °C), high quenching efficiency (>90%) for various fluorophores (*e.g.*, FAM, Cy5, and ROX), and large surfaces for simultaneous assembly of different DNA strands. We further show that silicon-based nanoMBs are highly effective for sensitive and specific multidetection of DNA targets. The unprecedented advantages of silicon-based multicolor nanoMBs would bring new opportunities for challenging bioapplications, such as allele discrimination, early cancer diagnosis, and molecular engineering, *etc.*

KEYWORDS: molecular beacons · silicon nanowires · gold nanoparticles · DNA · multianalysis

Molecular beacons (MBs) are specifically designed stem-loop-structured oligonucleotides that are dually labeled with a fluorophore−quencher pair at their opposite ends, enabling real-time analysis of target nucleic acids *via* observation of fluorescence alteration.[1] Since the introduction by Tyagi and Kramer in 1996, MBs have been extensively investigated as exceptional biomolecular probes and widely used for bioapplications (*e.g.*, biosensors, biochips, monitoring of living systems, *etc.*).[2−4] In principle, the stem helix brings the quencher and fluorophore into close proximity, leading to static fluorescence quenching. In the presence of the target molecule (*e.g.*, DNA or RNA), hybridization between the target and the loop sequence of the MB takes place, forcing the MB to undergo a spontaneous conformational change. As a result, fluorescence is restored due to spatial separation of the fluorophore and quencher. As is well-known, the quencher plays a critically important role in MBs as it may lead to higher quenching efficiency and a lower "OFF" signal. Organic molecules (*e.g.*, 4-{[4′-(dimethylamino)phenyl]azo}benzoic acid (DABCYL)), as conventional quenchers, have been well-established for construction of MBs. However, they often suffer from low quenching efficiency and variant quenching efficiency for different kinds of fluorophores. For example, while DABCYL efficiently quenches the fluorescence of carboxyfluorescein (FAM), they possess much less quenching efficiency for other kinds of dyes (*e.g.*, cyanine 5 (Cy5) and Texas red). Consequently, conventional MBs generally possess low sensitivity, and multicolor MBs for multianalysis are difficult to design.[1−6]

In recent years, a variety of nanomaterial-based molecular beacons (nanoMBs) composed of nanomaterials as quenchers have been developed.[1,7−12] For example, gold nanoparticle (AuNP)-based nanoMBs have been shown to be highly efficient for sensitive DNA detection because AuNPs could quench fluorophores with 100-fold higher efficiency than organic quenchers.[7−9] More recently, carbon nanotubes (CNTs) and graphene, as novel quenchers, have

* Address correspondence to apannale@cityu.edu.hk (S.T.L.), fchh@sinap.ac.cn (C.F.), yaohe@suda.edu.cn (Y.H.).

Received for review December 23, 2011 and accepted February 13, 2012.

Published online February 13, 2012
10.1021/nn2050449

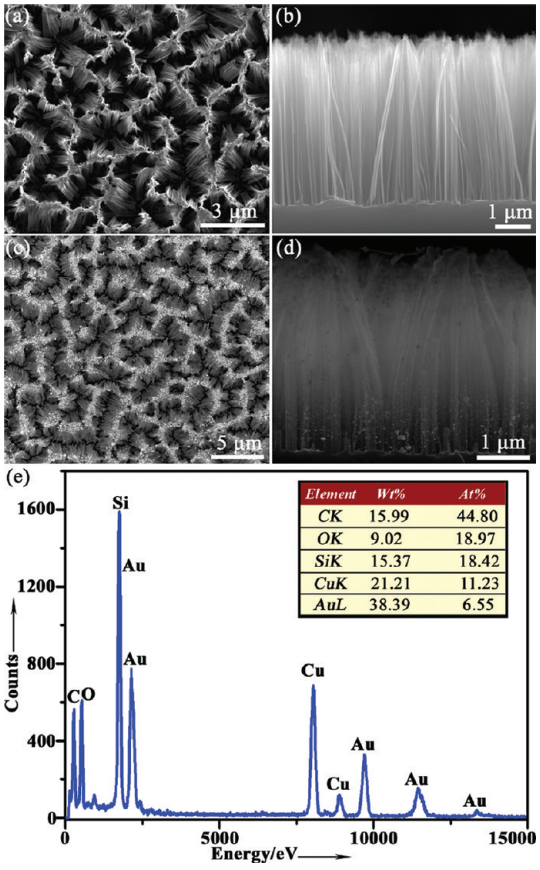

Figure 1. Top (a) and cross-section (b) scanning electronic microscopy (SEM) images of the free SiNW arrays. Top (c) and cross-section (d) SEM images of the AuNP-decorated SiNW arrays. (e) EDX pattern of the AuNP-decorated SiNW samples; presents the corresponding elemental ratio calculated by the EDX software, revealing that the as-prepared AuNP-decorated SiNWs contain Si and Au with 18.42 and 6.55% atomic concentration and 18.79% O due to oxidation of SiNWs in the ambient environment. Note that C and Cu weight concentration listed in the table are not available since carbon-based copper grids were used for the EDX test.[18−20,25]

been used to design nanobeacons with high sensitivity. Moreover, multicolor MBs were possible since fluorescence of different kinds of dyes could be efficiently quenched by CNTs and graphene.[10−12] Nevertheless, those AuNP-based nanobeacons generally possess poor salt stability and thermostability, thus limiting their wide applications.[7,9,13] Further, DNA is prone to nonspecifically adsorb on CNTs or graphene *via* $\pi-\pi$ stacking interaction, leading to poor detection specificity of the CNT- or graphene-based nanoMBs.[7,10−12] Recently, differently sized quantum dots functionalized with different nucleic acids were employed for multiplexed detection of different DNA targets.[14] Despite the progress, there is still remaining a big challenge to develop high-performance nanoMBs with robust stability and high sensitivity and selectivity.

Silicon nanomaterials are an important nanostructure and have been extensively studied due to their attractive properties, such as excellent electronic/mechanical/optical properties, favorable biocompatibility, surface tailorability, and compatibility with conventional silicon technology, *etc.*[15−20] Particularly, silicon nanowires (SiNWs), as a type of most important one-dimensional silicon nanostructures, have shown great promise for various applications ranging from electronics to biology (*e.g.*, solar cells, catalysts, sensors, antimicrobials, and bioimaging).[21−29] Of particular note, silicon-based nanohybrids made of SiNWs decorated with nanoparticles (NPs) with remarkable properties have been intensively studied recently.[21−26] For instance, silver nanoparticle (AgNP)-decorated SiNWs show ultrahigh surface-enhanced Raman scattering and antibacterial activity, which are distinctly superior to free AgNPs.[22−24] Fluorescent quantum dot (QD)-decorated SiNWs possess much stronger photostability compared to that of free QDs.[25] Those attractive properties strongly suggest SiNWs as a promising platform for the design of high-performance SiNW-based nanohybrids with unique merits. On the basis of previous achievements, we herein report the first example of silicon-based multicolor nanoMBs, made by using AuNP-decorated silicon nanowires (AuNP@SiNW) as high-performance quenchers. Significantly, such SiNW quenchers feature robust stability in high-concentration (0.1 M) salt solution and wide-ranging temperature (10−80 °C), as well as high quenching efficiency (>90%) for a range of fluorophores (*e.g.*, FAM, Cy5, and ROX). Consequently, silicon-based nanoMBs are shown to be superbly suitable for sensitive and specific multianalysis of DNA.

RESULTS AND DISCUSSION

Free SiNW arrays with ~170 nm diameter and ~4 μm length are first produced *via* a well-established HF-assisted etching (HAE) method (Figure 1a,b), developed in our previous reports.[30−32] Thereafter, AuNPs are readily coated on the surface of SiNWs through a reduction reaction based on established protocols,[22,24,26] producing the AuNP@SiNW array (Figure 1c,d). Energy-dispersive X-ray spectroscopy (EDX) and corresponding elemental ratio analysis confirm the presence of gold (~39% weight concentrations) in the AuNP@SiNW (Figure 1e). The resultant AuNP@SiNW arrays are then detached from the surface of the Si wafer by ultrasonic treatment and collected for design of silicon-based nanoMBs in our following experiment. Transmission electronic microscopy (TEM) images (Figure 2a) of the AuNPs@SiNWs show that about ~2600 AuNPs with sizes of 8−20 nm are distributed on SiNWs with a diameter of ~170 nm and length of ~2 μm.

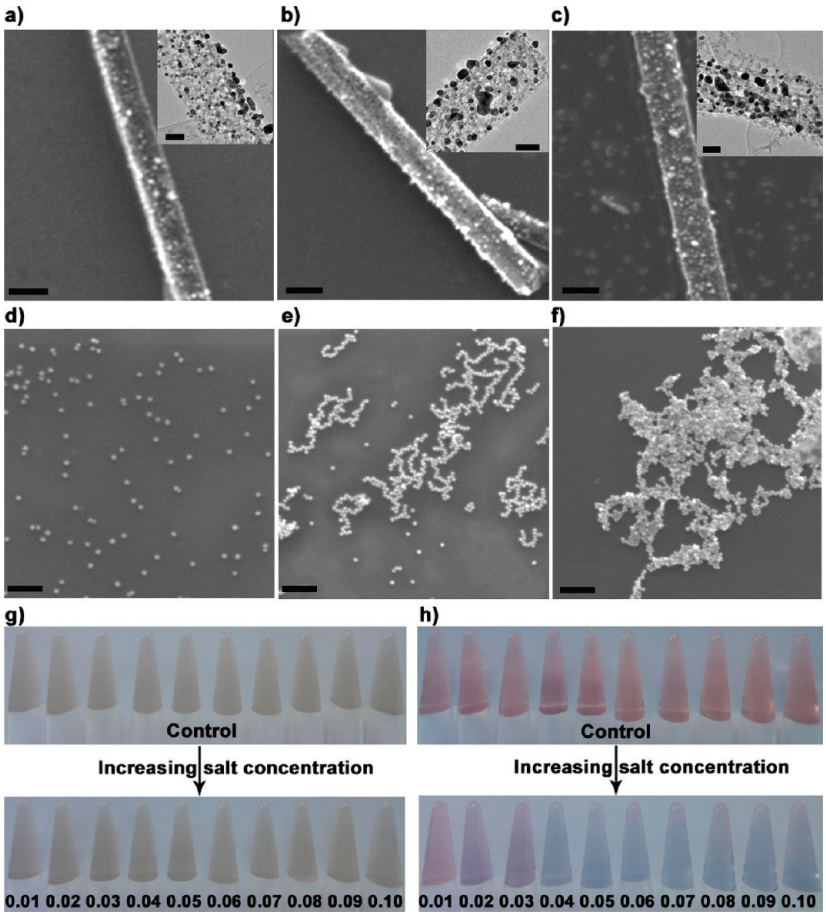

Figure 2. SEM images of AuNP-decorated SiNWs (a−c) and free AuNPs (d−f) in NaCl aqueous solution with different concentrations (from left to right: 0, 0.03, and 0.08 M). Bar: 200 nm. Insets in (a−c) show TEM images of AuNP-decorated SiNWs. Bar: 50 nm. (g,h) Display digital images of the AuNP-decorated SiNWs or free AuNP solution with NaCl concentrations increasing from 0.01 to 0.1 M as marked.

Salt stability is of particular importance for nanoMB-relative applications (*e.g.*, aging process in salt solution is required for DNA assembly with nanoMBs).[9,13] Significantly, the resultant AuNP@SiNW possesses robust stability in aqueous solution of a wide range of salt concentrations (0.01−0.1 M). As shown in Figure 2d−f, while free AuNPs (recognized as established nanoquenchers) are stable in aqueous solution (Figure 2d), they gradually become aggregated with increasing salt concentrations (Figure 2e,f), due to salt-induced reduction of electrostatic repulsion between AuNPs.[8] In striking contrast, for AuNPs@SiNWs, no obvious aggregation of AuNPs is observed, even in solutions with salt concentration as high as 0.08 M (Figure 2a−c). Figure 1g shows that AuNPs@SiNWs form a stable light-brown colloidal suspension in salt solutions of various concentrations. This is in sharp contrast to the free AuNP solution, whose color is distinctly changed from red to blue with increasing salt concentration from 0.01 to 0.1 M (Figure 2h), indicating salt-induced severe aggregation of AuNPs.[13,33−35] It provides further demonstration of the superior salt stability of AuNPs@SiNWs. We attribute the robust salt stability to SiNWs serving as an effective substrate for binding to the *in situ* AuNPs, effectively preventing aggregation of AuNPs.[24,25,36,37]

TABLE 1. Quenching Efficiency of Free-Standing SiNWs and AuNP-Decorated SiNWs

	free SiNWs (%)	AuNPs@SiNWs (%)
FAM	91.5	93.2
Cy5	97.1	96.3
ROX	96.4	96.7

In addition to robust salt stability, the resultant AuNPs@SiNWs feature ultrahigh fluorescence quenching efficiency (>93%, Table 1) toward a variety of organic fluorophores. Quenching efficiency (QE) is calculated using the equation[8−12]

$$QE = (I_{dye} - I_{SiNWs})/(I_{dye}) \quad (1)$$

where I_{dye} and I_{SiNWs} are the fluorescence intensity of the organic dyes and SiNWs/AuNPs@SiNWs, which are estimated based on fluorescence spectra of different dyes quenched by free SiNWs and AuNPs@SiNWs. As shown in Figure 3, fluorescence of three kinds of conventional organic dyes, such as FAM (carboxyfluorescein),

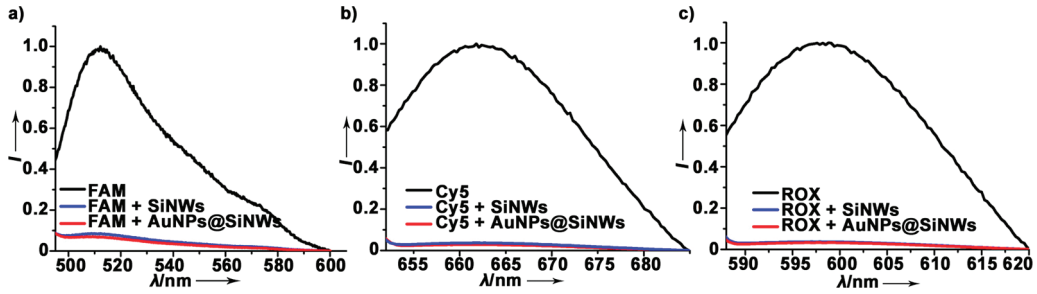

Figure 3. Fluorescence spectra of different dyes, such as FAM (a), Cy5 (b), and ROX (c), quenched by free SiNWs and AuNPs@SiNWs of the same concentrations (1.55 μg/mL). Fluorescence of three kinds of organic dyes almost disappeared in the presence of the free SiNWs or AuNPs@ SiNWs.

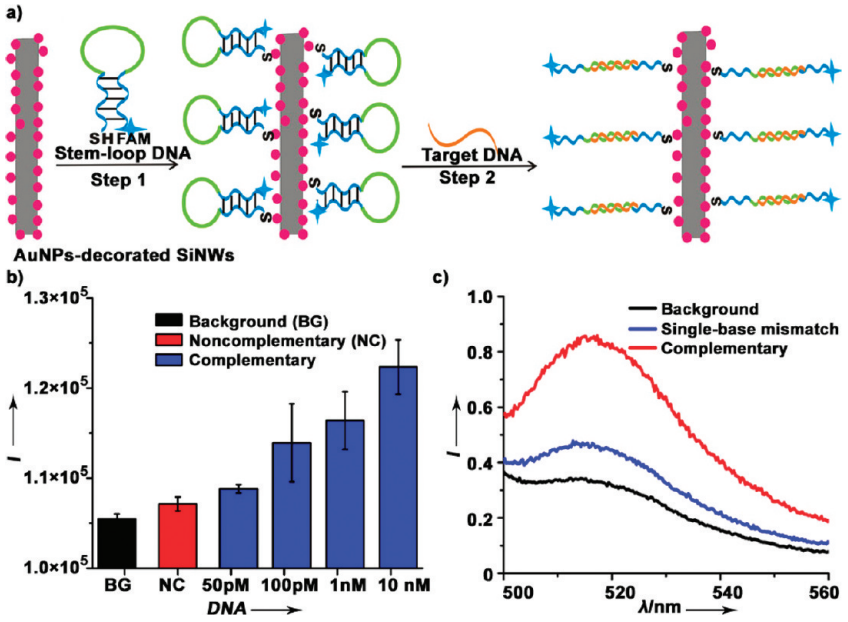

Figure 4. (a) Schematic preparation of silicon-based nanoMBs for DNA analysis (figure is not to scale). (b) Fluorescence intensity of different concentrations of complementary target DNA. Background and noncomplementary sequence are presented as control. (c) Photoluminescence spectra of FAM-tagged probes in the absence and presence of 10 nM complementary target DNA and single-based mismatched DNA ($\lambda_{excitation}$ = 480 nm).

Cy5 (cyanine 5), and ROX (6-carboxy-X-rhodamine), almost disappeared completely in the presence of the AuNPs@SiNWs. Moreover, control experiment shows that free SiNWs (SiNWs without surface modification) possess similarly high quenching efficiency (>90%, Table 1) for the three kinds of organic dyes. We attribute such high quenching efficiency to efficient long-range energy transfer from the dyes to SiNWs, similar to that in the reported AuNPs or CNTs (~90%).[8−10] Besides, the nanowire-based structures are favorable for enhancing charge transport, which is regarded as an additional contributor to the high quenching efficiency of SiNWs.[38−40]

It is worth pointing out that additional post-treatment (*e.g.*, O_2 plasma) and chemical reagents (*e.g.*, 3-(aminopropyl)triethoxysilane, APTES) are required for DNA assembly on surface of free SiNWs.[41−44] In contrary, DNA could be readily linked with the AuNPs@SiNWs *via* S−Au bonds based on established protocols, producing a DNA−AuNPs@SiNWs complex.[7−9,35] Therefore, the AuNPs@SiNWs with robust salt stability and high quenching efficiency are employed as quenchers to construct silicon-based nanoMBs for sensitive and specific detection of DNA. As shown in Figure 4a, stem-loop-structured DNA strands, whose opposite ends are modified with FAM and thiol molecules, are first assembled with the AuNP-decorated SiNWs *via* Au−S bonds, achieving silicon-based nanoMBs (step 1). Notably, the resultant nanoMBs produce feeble fluorescence since FAM molecules are close to the AuNPs@SiNWs (see background (BG) in Figure 4b,c). Once the target DNA is added, hybridization between the target and the loop sequence of the MB takes place, and the stronger intermolecular hybridization opens the weaker stem helix, leading to spatial separation of the organic dyes and AuNPs@SiNWs (Table 2). As a result, fluorescence is largely restored in the presence of target DNA (step 2).[1−4] In our experiment, target DNA with a series of concentrations is readily detected *via* the

TABLE 2. Oligonucleotide Sequences for DNA Detection by Using the Silicon-Based nanoMBs (See Schematic Route in Figure 3a)

oligonucleotides	sequences
stem-loop DNA probe	5′-FAM-CGCTC[a] CCT TAT TAT TAT TCC GAGCG[a]-T10[b]-$(CH_2)_6$-SH-3′
target DNA 1 (perfectly matched)	5′-GGA ATA ATA ATA AGG-3′
target DNA 2 (single-base mismatched)	5′-GGA ATA AC[c]A ATA AGG-3′
noncomplementary DNA 3	5′-TGA GTG GAC GTC AAC GAG CAA-3′

[a] Underlined letters represent the stem sequence. [b] T10 represents 10 Ts that serve as the spacer. [c] Italic letter represents the mismatched site.

TABLE 3. Oligonucleotide Sequences for Multidetection of Three Types of Tumor-Suppressor Genes (p16, p21, and p53) by Using the Silicon-Based NanoMBs (See Schematic Route in Figure 4a)

oligonucleotides	sequences
stem-loop DNA probe A (p16)	5′-FAM-CGCTC[a] CAG AGG CAG TAA CCA GAGCG[a]-T10[b]-$(CH_2)_6$-SH-3′
target DNA A (p16 gene segment)	5′-TGG TT A CTG CCT CTG-3′
target DNA A′ (single-base mismatch)	5′-TGG TT A CC[c]G CCT CTG-3′
stem-loop DNA probe B (p21)	5′-Cy5-CGCTC[a] CCC TAA TCC GCC CAC GAGCG[a]-T10[b]-$(CH_2)_6$-SH-3′
target DNA B (p21 gene segment)	5′-GTG GGC GGA TTA GGG-3′
target DNA B′ (single-base mismatch)	5′-GTG GGC GT[c]A TTA GGG-3′
stem-loop DNA probe C (p53)	5′-ROX-CGCTC[a] CCT GGT GCC GTA GAT GAGCG[a]-T10[b]-$(CH_2)_6$-SH-3′
target DNA C (p53 gene segment)	5′-ATC TAC GGC ACC AGG-3′
target DNA C′ (single-base mismatched)	5′-ATC TAC GC[c]C ACC AGG-3′

[a] Underlined letters represent the stem sequence. [b] T10 represents 10 Ts that serve as the spacer. [c] Italic letters represent the mismatched site.

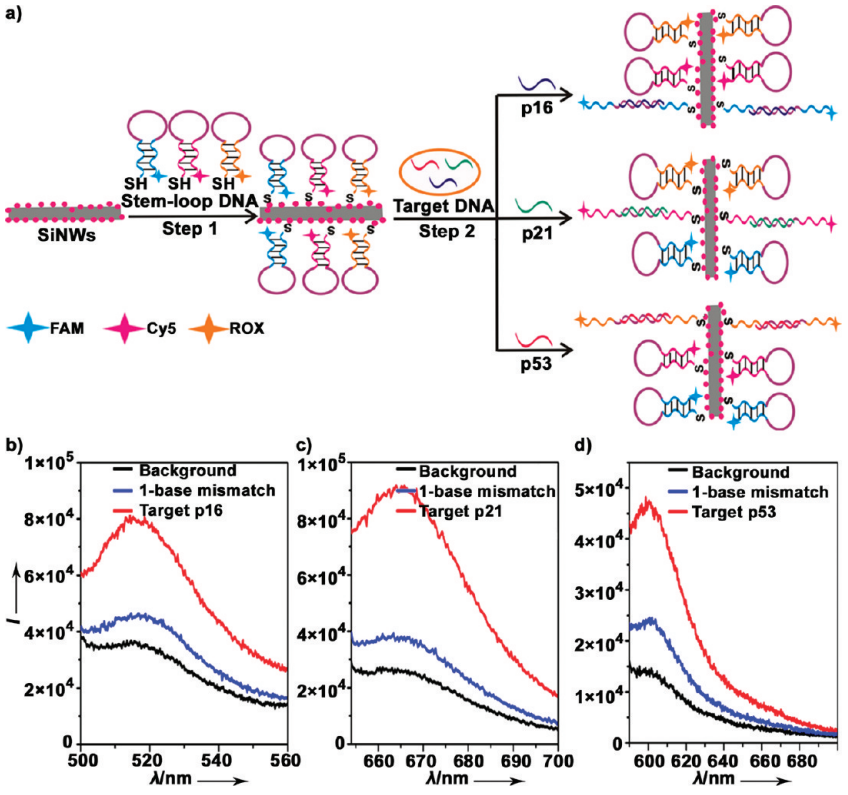

Figure 5. (a) Schematic preparation of silicon-based multicolor nanoMBs for DNA multianalysis (figure is not to scale). (b–d) Fluorescence spectra for multicolor Si-based nanobeacons in the presence of 10 nM target DNA or single-base mutated gene, (b) FAM-tagged p16 with maximum emission wavelength at 516 nm ($\lambda_{excitation}$ = 480 nm), (c) Cy5-tagged p21 with maximum emission wavelength at 661 nm ($\lambda_{excitation}$ = 643 nm), and (d) ROX-tagged p53 with maximum emission wavelength at 605 nm ($\lambda_{excitation}$ = 598 nm).

recording intensity of fluorescence recovery. As shown in Figure 4b, fluorescence intensity is gradually enhanced with increasing DNA concentrations from 50 pM to 10 nM. Notably, the intensity of 100 pM target DNA

(~114 000) is distinctively larger than that of background (~105 000) or noncomplementary DNA (~107 000). It shows that the silicon-based nanoMBs enable the detection of DNA at low concentrations (~pM), better than the reported DNA detection limit (typically in the nanomolar range) by other kinds of nanoMBs (*e.g.*, AuNPs).[8−12] Furthermore, the nanoMBs are utilized for discrimination of single-base mismatch. Figure 4c shows that single-base mismatched DNA produces ~20% of the fluorescence intensity (with background subtracted) of the fully complementary target, demonstrating that silicon nanoMBs retain high sequence specificity offered by the conformational constraint of stem-loop structures.[2,7,9]

Simultaneous multicolor detection of targets is important for molecular diagnostics. For example, early phase cancers have been proven to be associated with multiple tumor-suppressor genes.[45,46] Large surface of the AuNP-decorated SiNWs is available for assembling multiple DNA strands, thus affording the possibility to design all-in-one multicolor nanoMBs.[1] Indeed, three kinds of hairpin DNA probes labeled with FAM, Cy5, or ROX are readily assembled on the surface of one single SiNW in our experiment. The resultant multicolor nanoMBs are then employed for simultaneous multidetection of three types of tumor-suppressor genes, that is, exon segments of p16, p21, and p53 genes (Table 3).[47−49] The nanoMBs stay in the "OFF" state and produce feeble fluorescence in the absence of target DNA (black lines in Figure 5b−d). Upon the addition of specific targets to the probe mixture p16, p21, and p53, the fluorescence intensity of nanobeacons is significantly enhanced. Notably, the nanoMBs emit at the unique wavelengths in response to the specific targets because dye-to-dye energy transfer is effectively avoided due to distinctly different maximum emission wavelengths of the three dyes (red lines in Figure 5b−d). Notably, the concentration of target DNA used for multiplex analysis is as low as 10 nM, which is comparable or superior to the detection limit (5−50 nm) of well-established nanoMBs (*e.g.*, AuNPs and graphene).[9,11] Moreover, for the single-base mismatched DNA, the fluorescence intensity is restored to some extent and reaches 20.1, 19.2, or 28.4% of the intensity of the complementary DNA for p16, p21, or p53, respectively (blue lines in Figure 5b−d). These results suggest that the resultant silicon-based multicolor nanoMBs are superbly suitable for concurrent analysis of multiple gene targets.

Kinetic and thermodynamic properties of the silicon-based nanoMBs are further investigated. As shown in Figure 6a, nanoMBs stay in "close" state in the absence of target (black line) but fluoresce upon meeting the specific target. Particularly, fluorescence of nanoMBs is restored and enhanced to ~30% within 5 min (red line). This kinetics is similar to the established

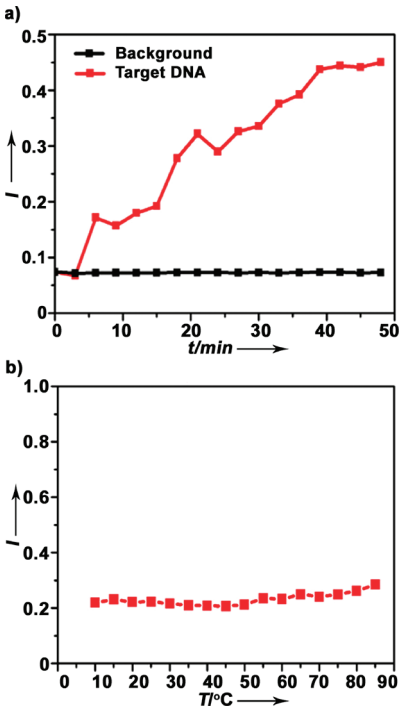

Figure 6. Kinetic and thermodynamic properties of silicon-based nanoMBs. (a) Time-dependent fluorescence change of silicon-based nanoMBs in the absence or presence of different concentrations of FAM-tagged target DNA (100 pM). (b) Temperature effects on fluorescence of silicon-based nanoMBs ($\lambda_{excitation}$ = 480 nm).

AuNP-based nanoMBs (*ca.* ~40% within 5 min) but lower than that of conventional stem-loop MBs (*ca.* ~80% within 5 min).[2,7] We reason that the strong affinities of fluorophore binding to AuNPs@SiNWs would reduce the rates of hybridization and loop opening, similar to the reported mechanism of AuNP-based nanoMBs.[8,9] Notwithstanding, this minute-level kinetic is rapid enough to meet the criteria for various practical applications.[1,7] In addition, thermostability of the silicon-based nanoMBs is studied by monitoring the fluorescence change over a temperature profile. Significantly, the prepared nanoMBs show extremely strong temperature stability, preserving feeble fluorescence in a wide range of temperature from 10 to 80 °C (Figure 6b), which is superior to the conventional MBs or established AuNP nanoMBs (*e.g.*, while both kinds of MBs are held in the "close" state with minimal fluorescence at low temperature (20−40 °C), their fluorescence is obviously restored along with temperature elevation due to their thermal destabilization[8,9]). This unique behavior indicates that the AuNPs@SiNWs undergo little or no conformational changes in the temperature range studied, and surface adsorption is much less dependent on temperature than DNA melting.[8,50] It is worth pointing out that such remarkable thermal stability allows the use of the silicon-based nanoMBs in various temperature-relevant applications, such as real-time PCR studies under normal temperature-cycling conditions.[51,52]

CONCLUSION

To summarize, we have presented a novel multicolor silicon-based nanoMBs by using AuNPs@SiNWs as high-performance quenchers. Significantly, the nanoMBs feature robust salt and thermal stability, high quenching efficiency to various kinds of fluorophores, and large surface for concurrent assembly of different DNA strands. Our findings further demonstrate that the silicon-based nanoMBs are highly effective for sensitive and specific multidetection of DNA targets. Consequently, silicon-based multicolor nanoMBs, serving as promising molecular probes, can offer new opportunities for wide-ranging bioapplications, such as allele discrimination, early cancer diagnosis, and molecular engineering.[53]

METHODS

Materials and Devices. DNA oligonucleotides were synthesized and purified by TAKARA Biotechnology (Dalian, China). Hydrofluoric acid (≥40%), hydrogen peroxide (≥30%), silver nitrate (≥99.8%), nitric acid (65−68%), and gold chloride (≥47.8%) were purchased from Sinopharm Chemical Reagent Co., Ltd. (Shanghai, China). Silicon (100) wafer (phosphate-doped (p-type), 0.01−0.02 Ω sensitivity) was purchased from Heifei Kejing Materials Technology Co., Ltd. (China). All chemicals were used without additional purification. All solutions were prepared using Milli-Q water (Millipore) as the solvent. All optical measurements were performed at room temperature under ambient air conditions. UV−vis absorption spectra were recorded with a Perkin-Elmer Lambda 750 UV−vis−near-infrared spectrophotometer. Photoluminescence (PL) measurements were performed using a HORIBA JOBTN YVON FLUOROMAX-4 spectrofluorimeter. The TEM/HRTEM overview images were recorded using Philips CM 200 electron microscope operated at 200 kV. SEM was characterized by using scanning electron microscopy (FEI Quanta 200F). Energy-dispersive X-ray (EDX) spectroscopy was utilized to determine the fraction of the resultant AuNP-decorated SiNWs. The samples were first dispersed onto carbon-coated copper grids with the excess solvent evaporated and then characterized by using Philips CM 200 electron microscope equipped with EDX spectroscopy.

Synthesis of AuNPs@SiNWs. Basically, SiNW arrays were produced *via* a well-established HF-assisted etching (HAE) method, developed in our previous reports.[30−32] In detail, the silicon wafer was cleaned with acetone by ultrasonic treatment for 10 min and washed with Milli-Q water (Millipore) three times. Afterward, the silicon wafer was immersed in an oxidant solution containing H_2SO_4 (98%) and H_2O_2 (30%) with a volume ratio of 3:1 for 30 min and rinsed with Milli-Q water three times to remove organics. The cleaned silicon wafer was further immersed in hydrogen fluoride (HF, 5%) aqueous solution for 30 min to achieve a fresh H-terminated silicon wafer covered by Si−H bonds. The H-terminated silicon wafer was then immediately placed into a freshly prepared reduction solution containing silver nitrate ($AgNO_3$) and HF (10%) and slowly stirred for 3 min. Thereafter, the treated silicon wafer was immersed into a solution composed of 10% HF and 0.4 M H_2O_2 for 5 min, achieving the aligned SiNWs with ∼170 nm diameter and ∼4 μm length. Afterward, the resultant aligned SiNWs were immersed into 1 mM $HAuCl_4$ for 5 min at 60 °C, rinsed with ultrapure water three times, and dried under a stream of N_2. AuNPs were readily coated on the surface of SiNWs through a reduction reaction, producing the AuNP@SiNW array. The resultant AuNP@SiNW arrays were then detached from the surface of the Si wafer by ultrasonic treatment and collected for design of silicon-based nanoMBs.

Construction of Silicon-Based NanoMBs. The whole procedure is schematically shown in Figure 4a. In detail, 1.55 mg of the resultant AuNPs@SiNWs was first dispersed in 50 mL of aqueous solution, achieving a AuNPs@SiNWs solution with a concentration of 31 μg/mL. Afterward, 10 μL of 1 μM fluorophore-tagged loop-structured DNA was added to a 1 mL solution of AuNPs@SiNWs, which was then kept in a sealed box overnight. One molar NaCl phosphate-buffered solution was added to the mixture to yield a final concentration of 0.1 M NaCl for 12 h to guarantee adequate self-assembly between DNA and AuNPs@SiNWs. The resultant product was precipitated *via* centrifugation at 12 000 rpm for 15 min at 4 °C and then washed three times with 100 mM PBS solution (pH 7.0), with repetitive centrifugation and dispersion. The final product was collect as silicon-based nanoMBs for further DNA detection.

DNA Detection by Using the Silicon-Based MBs. Manipulation is similar to that of AuNP-based MBs described in our previous publication.[9] The resultant MBs were hybridized with the target DNA (10 μL, 1 μM) in 1 mL of hybridization buffer (10 mM Tris·HCl, pH 8.0, 100 mM KCl, 1 mM $MgCl_2$) for 30 min at 37 °C. The fluorescence recovery of nanoMBs was monitored in a spectrofluorimeter.

The manipulations were repeated for target DNA with different concentration in the range of 50 pM to 10 nM. When single-base mismatched DNA was used, all of the manipulations were identical to those described above.

For multidetection of three types of tumor-suppressor genes (*i.e.*, exon segments of p16, p21, and p53 genes), multicolor nanoMBs containing FAM, ROX, and Cy5 colors were employed. Either complementary or one-base mismatched DNA targets of different origins were spiked in a 1 mL hybridization buffer containing multicolor nanoMBs. After 30 min incubation, the fluorescence was monitored at appropriate excitation wavelengths. The FAM fluorescence was excited at 480 nm and measured at 512 nm; the ROX fluorescence was excited at 578 nm and measured at 598 nm, and the Cy5 fluorescence of was excited at 643 nm and measured at 661 nm.

Salt Stability Comparison of Free AuNPs and AuNP-Decorated SiNWs. The salt stability of AuNPs and AuNPs@SiNWs was investigated by adding NaCl of different concentrations. Samples under salt circumstances were characterized by the UV−vis and SEM. One molar NaCl was added to the 100 μL sample solution to reach a final concentration of 0.01−0.1 M. The mixed solution was further incubated for a few seconds. Notably, the free-standing AuNPs are gradually aggregated by adding NaCl solution, whose color is distinctly changed from pink to purple (0−0.03 M NaCl) and eventually to blue (0.04−0.1 M NaCl). In contrast, the color of SiNWs@AuNPs did not change after adding NaCl solution, even in high salt solution (*e.g.*, 0.1 M NaCl), suggesting that SiNWs@AuNPs were stable in salt solution.

Kinetic and Thermodynamic Studies of Silicon-Based MBs. DNA targets of 100 nM were employed in both kinetic and thermodynamic studies. For kinetic and time-dependent studies, a series of fluorescence spectra were acquired at 3 min time intervals, and the peak intensity at 512 nm was plotted as a function of time. All of the spectra were obtained at room temperature by excitation with a 480 nm excitation wavelength. For thermodynamic studies, fluorescence intensity was monitored at temperatures varied from 10 to 85 °C, with a 5 °C elevation each step of 5 min incubation.

Conflict of Interest: The authors declare no competing financial interest.

Acknowledgment. This work was supported by National Basic Research Program of China (973 Program 2012CB932400, 2012CB932600), NSFC (30900338, 51072116), Research Grants Council of Hong Kong SAR, China - CRF Grant (No. CityU5/CRF/08) and GRF Grant (No. CityU102010), and a Project Funded by the Priority Academic Program Development of Jiangsu Higher Education Institutions (PAPD).The authors thank Prof. L.S. Liao for fruitful discussions.

REFERENCES AND NOTES

1. Wang, K. M.; Tang, Z. W.; Yang, C. Y. J.; Kim, Y. M.; Fang, X. H.; Li, W.; Wu, Y. R.; Medley, C. D.; Cao, Z. H.; Li, J.; *et al.* Molecular Engineering of DNA: Molecular Beacons. *Angew. Chem., Int. Ed.* **2009**, *48*, 856–870.
2. Tyagi, S.; Kramer, F. R. Molecular Beacons: Probes That Fluoresce upon Hybridization. *Nat. Biotechnol.* **1996**, *14*, 303–308.
3. Tyagi, S.; Marras, S. A. E.; Kramer, F. R. Wavelength-Shifting Molecular Beacons. *Nat. Biotechnol.* **2000**, *18*, 1191–1196.
4. Heyduk, T.; Heyduk, E. Molecular Beacons for Detecting DNA Binding Proteins. *Nat. Biotechnol.* **2002**, *20*, 171–176.
5. Tyagi, S.; Bratu, D. P.; Kramer, F. R. Multicolor Molecular Beacons for Allele Discrimination. *Nat. Biotechnol.* **1998**, *16*, 49–53.
6. Dubertret, B.; Calame, M.; Libchaber, A. J. Single-Mismatch Detection Using Gold-Quenched Fluorescent Oligonucleotides. *Nat. Biotechnol.* **2001**, *19*, 365–370.
7. Song, S. P.; Qin, Y.; He, Y.; Huang, Q.; Fan, C. H.; Chen, H. Y. Functional Nanoprobes for Ultrasensitive Detection of Biomolecules. *Chem. Soc. Rev.* **2010**, *39*, 4234–4243.
8. Maxwell, D. J.; Taylor, J. R.; Nie, S. M. Self-Assembled Nanoparticle Probes for Recognition and Detection of Biomolecules. *J. Am. Chem. Soc.* **2002**, *124*, 9606–9612.
9. Song, S.; Liang, Z.; Zhang, J.; Wang, L.; Li, G.; Fan, C. H. Gold-Nanoparticle-Based Multicolor Nanobeacons for Sequence-Specific DNA Analysis. *Angew. Chem., Int. Ed.* **2009**, *48*, 8670–8674.
10. Yang, R.; Jin, J.; Chen, Y.; Shao, N.; Kang, H.; Xiao, Z.; Tang, Z.; Wu, Y.; Zhu, Z.; Tan, W. H. Carbon Nanotube-Quenched Fluorescent Oligonucleotides: Probes That Fluoresce upon Hybridization. *J. Am. Chem. Soc.* **2008**, *130*, 8351–8358.
11. He, S. J.; Song, B.; Li, D.; Zhu, C.; Qi, W.; Wen, Y.; Wang, L.; Song, S.; Fang, H.; Fan, C. H. Graphene Nanoprobes for Rapid, Sensitive, and Multicolor Fluorescent DNA Analysis. *Adv. Funct. Mater.* **2010**, *20*, 453–459.
12. Lu, C. H.; Yang, H. H.; Zhu, C. L.; Chen, X.; Chen, G. N. A Graphene Platform for Sensing Biomolecules. *Angew. Chem., Int. Ed.* **2009**, *121*, 4879–4881.
13. Elghanian, R.; Storhoff, J. J.; Mucic, R. C.; Letsinger, R. L.; Mirkin, C. A. Selective Colorimetric Detection of Polynucleotides Based on the Distance-Dependent Optical Properties of Gold Nanoparticles. *Science* **1997**, *277*, 1078–1081.
14. Freeman, R.; Liu, X. Q.; Willner, I. Chemiluminescent and Chemiluminescence Resonance Energy Transfer (CRET) Detection of DNA, Metal Ions, and Aptamer−Substrate Complexes Using Hemin/G-Quadruplexes and CdSe/ZnS Quantum Dots. *J. Am. Chem. Soc.* **2011**, *133*, 11597–11604.
15. Pavesi, L.; Negro, L. D.; Mazzoleni, C.; Franzo, G.; Priolo, F. Optical Gain in Silicon Nanocrystals. *Nature* **2000**, *408*, 440–444.
16. Ding, Z. F.; Quinn, B. M.; Haram, S. K. P.; Lindsay, E.; Korgel, B. A.; Bard, A. J. Electrochemistry and Electrogenerated Chemiluminescence from Silicon Nanocrystal Quantum Dots. *Science* **2002**, *296*, 1293–1297.
17. Patolsky, F.; Timko, B. P.; Yu, G. H.; Fang, Y.; Greytak, A. B.; Zheng, G. F.; Lieber, C. M. Detection, Stimulation, and Inhibition of Neuronal Signals with High-Density Nanowire Transistor Arrays. *Science* **2006**, *313*, 1100–1104.
18. He, Y.; Su, Y. Y.; Yang, X. B.; Kang, Z. H.; Xu, T. T.; Zhang, R. Q.; Fan, C. H.; Lee, S. T. Photo and pH Stable, Highly-Luminescent Silicon Nanospheres and Their Bioconjugates for Immunofluorescent Cell Imaging. *J. Am. Chem. Soc.* **2009**, *131*, 4434–4438.
19. He, Y.; Kang, Z. H.; Li, Q. S.; Tsang, C. H. A.; Fan, C. H.; Lee, S. T. Ultrastable, Highly Fluorescent, and Water-Dispersed Silicon-Based Nanospheres as Cellular Probes. *Angew. Chem., Int. Ed.* **2009**, *48*, 128–132.
20. He, Y.; Zhong, Y. L.; Peng, F.; Wei, X. P.; Su, Y. Y.; Lu, Y. M.; Su, S.; Gu, W.; Liao, L. S.; Lee, S. T. One-Pot Microwave Synthesis of Water-Dispersible, Ultraphoto and pH Stable, and Highly Fluorescent Silicon Quantum Dots. *J. Am. Chem. Soc.* **2011**, *133*, 14192–14195.
21. Ma, D. D. D.; Lee, C. S.; Au, F. C. K.; Tong, S. Y.; Lee, S. T. Small-Diameter Silicon Nanowire Surfaces. *Science* **2003**, *299*, 1874–1877.
22. Lv, M.; Su, S.; He, Y.; Huang, Q.; Hu, W. B.; Li, D.; Fan, C. H.; Lee, S. T. Long-Term Antimicrobial Effect of Silicon Nanowires Decorated with Silver Nanoparticles. *Adv. Mater.* **2010**, *22*, 5463–5467.
23. Peng, K. Q.; Lee, S. T. Silicon Nanowires for Photovoltaic Solar Energy Conversion. *Adv. Mater.* **2011**, *23*, 198–215.
24. He, Y.; Su, S.; Xu, T. T.; Zhong, Y. L.; Zapien, J. A.; Li, J.; Fan, C. H.; Lee, S. T. Silicon Nanowires-Based Highly-Efficient SERS-Active Platform for Ultrasensitive DNA Detection. *Nano Today* **2011**, *6*, 122–130.
25. He, Y.; Zhong, Y. L.; Peng, F.; Wei, X. P.; Su, Y. Y.; Su, S.; Gu, W.; Liao, L. S.; Lee, S. T. Highly Luminescent Water-Dispersible Silicon Nanowires for Long-Term Immunofluorescent Cellular Imaging. *Angew. Chem., Int. Ed.* **2011**, *50*, 3080–3083.
26. He, Y.; Fan, C. H.; Lee, S. T. Silicon Nanostructures for Bioapplications. *Nano Today* **2010**, *5*, 282–295.
27. Kim, W.; Ng, J. K.; Kunitake, M. E.; Conklin, B. R.; Yang, P. D. Interfacing Silicon Nanowires with Mammalian Cells. *J. Am. Chem. Soc.* **2007**, *129*, 7228–7229.
28. Jung, Y.; Tong, L.; Tanaudommongkon, A.; Cheng, J. X.; Yang, C. *In Vitro* and *In Vivo* Nonlinear Optical Imaging of Silicon Nanowires. *Nano Lett.* **2009**, *9*, 2440–2444.
29. Li, Z.; Song, J.; Mantini, G.; Lu, M. Y.; Fang, H.; Falconi, C.; Chen, L. J.; Wang, Z. L. Quantifying the Traction Force of a Single Cell by Aligned Silicon Nanowire Array. *Nano Lett.* **2009**, *9*, 3575–3580.
30. Peng, K. Q.; Yan, Y. J.; Gao, S. P.; Zhu, J. Synthesis of Large-Area Silicon Nanowire Arrays *via* Self-Assembling Nanoelectrochemistry. *Adv. Mater.* **2002**, *14*, 1164–1167.
31. Peng, K. Q.; Wu, Y.; Fang, H.; Zhong, X. Y.; Xu, Y.; Zhu, J. Uniform, Axial-Orientation Alignment of One-Dimensional Single-Crystal Silicon Nanostructure Arrays. *Angew. Chem., Int. Ed.* **2005**, *44*, 2737–2742.
32. Peng, K. Q.; Lu, A. J.; Zhang, R. Q.; Lee, S. T. Motility of Metal Nanoparticles in Silicon and Induced Anisotropic Silicon Etching. *Adv. Funct. Mater.* **2008**, *18*, 3026–3035.
33. Grabar, K. C.; Freeman, R. G.; Hommer, M. B.; Natan, M. J. Preparation and Characterization of Au Colloid Monolayers. *Anal. Chem.* **1995**, *67*, 735–743.
34. Li, H.; Rothberg, L. Colorimetric Detection of DNA Sequences Based on Electrostatic Interactions with Unmodified Gold Nanoparticles. *Proc. Natl. Acad. Sci. U.S.A.* **2004**, *101*, 14036–14039.
35. Zhang, J.; Song, S. P.; Wang, L. H.; Pan, D.; Fan, C. A Gold Nanoparticle-Based Chronocoulometric DNA Sensor for Amplified Detection of DNA. *Nat. Protoc.* **2007**, *2*, 2888–2895.
36. Chumanov, G.; Sokolov, K.; Gregory, B. W.; Cotton, T. M. Colloidal Metal Films as a Substrate for Surface-Enhanced Spectroscopy. *J. Phys. Chem.* **1995**, *99*, 9466–9471.
37. Freeman, R. G.; Grabar, K. C.; Allison, K. J.; Bright, R. M.; Davis, J. A.; Guthrie, A. P.; Hommer, M. B.; Jackson, M. A.; Smith, P. C.; Walter, D. G.; *et al.* Self-Assembled Metal Colloid Monolayers: An Approach to SERS Substrates. *Science* **1995**, *267*, 1629–1632.
38. Tsakalakos, L.; Balch, J.; Fronheiser, J.; Korevaar, B. A.; Sulima, O.; Rand, J. Silicon Nanowire Solar Cells. *Appl. Phys. Lett.* **2007**, *91*, 23317.
39. Gur, I.; Fromer, N. A.; Geier, M. L.; Alivisatos, A. P. Air Stable All-Inorganic Nanocrystal Solar Cells Processed from Solution. *Science* **2005**, *310*, 462–465.
40. Tian, B. Z.; Zheng, X. L.; Kempa, T. J.; Fang, Y.; Yu, N. F.; Yu, G. H.; Huang, J. L.; Lieber, C. Coaxial Silicon Nanowires as Solar Cells and Nanoelectronic Power Sources. *Nature* **2007**, *449*, 885–890.
41. Bunimovich, Y. L.; Shin, Y. S.; Yeo, W. S.; Amori, M.; Kwong, G.; Heath, J. R. Quantitative Real-Time Measurements of DNA Hybridization with Alkylated Nonoxidized Silicon Nanowires in Electrolyte Solution. *J. Am. Chem. Soc.* **2006**, *128*, 16323–16331.

42. Li, Z.; Chen, Y.; Li, X.; Kamins, T. I.; Nauka, K.; Williams, R. S. Sequence-Specific Label-Free DNA Sensors Based on Silicon Nanowires. *Nano Lett.* **2004**, *4*, 245–247.
43. Wu, C. C.; Ko, F. H.; Yang, Y. S.; Hsia, D. L.; Leea, B. S.; Su, T. S. Label-Free Biosensing of a Gene Mutation Using a Silicon Nanowire Field-Effect Transistor. *Biosens. Bioelectron.* **2009**, *25*, 820–825.
44. Zhang, G. J.; Chua, J. H.; Chee, R. E.; Agarwal, A.; Wong, S. M.; Buddharaju, K. D.; Balasubramanian, N. Highly Sensitive Measurements of PNA−DNA Hybridization Using Oxide-Etched Silicon Nanowire Biosensors. *Biosens. Bioelectron.* **2008**, *23*, 1701–1707.
45. Sidransky, D. Nucleic Acid-Based Methods for the Detection of Cancer. *Science* **1997**, *278*, 1054–1058.
46. Yokota, J. Tumor Progression and Metastasis. *Carcinogenesis* **2000**, *21*, 497–503.
47. Velculescu, V. E.; El-Deiry, W. S. Biological and Clinical Importance of the p53 Tumor Suppressor Gene. *Clin. Chem.* **1996**, *42*, 858–868.
48. Liggett, W. H., Jr.; Sidransky, D. Role of the p16 Tumor Suppressor Gene in Cancer. *J. Clin. Oncol.* **1998**, *16*, 1197–1206.
49. Kirla, R.; Salminen, E.; Huhtala, S.; Nuutinen, J.; Talve, L.; Haapasalo, H.; Kalimo, H. Prognostic Value of the Expression of Tumor Suppressor Genes p53, p21, p16 and prb, and Ki-67 Labelling in High Grade Astrocytomas Treated with Radiotherapy. *J. Neuro-Oncol.* **2000**, *46*, 71–80.
50. Bonnet, G.; Tyagi, S.; Libchaber, A.; Kramer, F. R. Thermodynamic Basis of the Enhanced Specificity of Structured DNA Probes. *Proc. Natl. Acad. Sci. U.S.A.* **1999**, *96*, 6171–6176.
51. Summerer, D.; Marx, A. A. Molecular Beacon for Quantitative Monitoring of the DNA Polymerase Reaction in Real-Time. *Angew. Chem., Int. Ed.* **2002**, *41*, 3620–3622.
52. Strerath, M.; Marx, A. Tuning PCR Specificity by Chemically Modified Primer Probes. *Angew. Chem., Int. Ed.* **2002**, *41*, 4766–4769.
53. Li, D.; Song, S. P.; Fan, C. H. Target-Responsive Structural Switching for Nucleic Acid-Based Sensors. *Acc. Chem. Res.* **2010**, *43*, 631–641.